

# Admittance memory cycles of Ta<sub>2</sub>O<sub>5</sub>-ZrO<sub>2</sub>-based RRAM devices

S. Dueñas, H. Castán, O. G. Ossorio, L. A. Domínguez, and H. García

Department of Electronics, University of Valladolid  
Valladolid, Spain  
sduenas@ele.uva.es

K. Kalam, and K. Kukli

Institute of Physics, University of Tartu, Estonia  
M. Ritala, and M. Leskelä  
Department of Chemistry, University of Helsinki  
Helsinki, Finland

**Abstract** — The resistive switching behavior of Ta<sub>2</sub>O<sub>5</sub>-ZrO<sub>2</sub>-based metal-insulator-metal devices was studied. Asymmetrical and repetitive current-voltage loops were observed. Excellent control of admittance parameters in the intermediate states between the high and low resistance ones was achieved, demonstrating suitability to analog and neuromorphic applications. Admittance memory cycles provide relevant information about the switching mechanism, in which the existence of two different metallic species in the dielectric seems to play an important role.

**Keywords**—Resistive memories, admittance memory cycles, Ta<sub>2</sub>O<sub>5</sub>:ZrO<sub>2</sub> ALD films

## I. INTRODUCTION

Nowadays the memristor devices, and specifically the resistive switching memories (RRAM), are attractive as a disruptive technology for novel information applications, due to extremely simple structure, fast speed, high scalability, and low power consumption. Hence, a great deal of work is being developed in order to study their endurance and repetitiveness characteristics. In the last years the capability of this kind of devices for the integration of information storage and processing has been pointed out as a possible solution of the von Neumann bottleneck problem in traditional computing architecture. The resistance in RRAMs is strongly dependent on the history of applied voltage values, which open an interesting way to emulate the biological synapse process. In fact, memristive devices are seen as potential building blocks for neuromorphic architectures. The majority of these devices are two-terminal MIM structures with a metal oxide between two proper metals. Among the potential switching materials, Ta<sub>2</sub>O<sub>5</sub> is a firm candidate in these fields (1-4) for its high dielectric constant (5) and high band gap (6). It has been demonstrated that the insertion of an interfacial layer could improve the memory characteristics of Ta<sub>2</sub>O<sub>5</sub>-based RRAM devices (7, 8).

The electrical tuning and control of capacitance between two clearly differentiate states could broaden the applications scope of RRAM devices, especially in the neuromorphic and analog arena. In comparison with the amount of studies focused on the

resistance changes, very few works in the literature deal with the study of the impedance parameters behavior (9, 10). Recently, we reported a detailed study of admittance cycles in HfO<sub>2</sub>-based RRAM devices with bipolar current-voltage loops (11). In this work we investigate the resistive switching behavior of Ta<sub>2</sub>O<sub>5</sub>:ZrO<sub>2</sub>-based MIM structures. In addition to the current-voltage measurements, we carry out a study of the small signal parameters, capacitance and conductance, which also show hysteretic loops. We demonstrate that it is possible to sense the memory state with a DC reading voltage of 0 V, that is, with no power composition. Moreover, we demonstrate that a continuum of internal states can be obtained depending on the stimulus amplitude. This fact is very interesting for analog and neural applications.

## II. EXPERIMENTAL SETUP

Amorphous Ta<sub>2</sub>O<sub>5</sub>-ZrO<sub>2</sub> films were grown on highly-doped conductive Si(100) substrates covered by 10 nm thick TiN films, in a flow-type hot-wall ALD reactor F120 at a substrate temperature of 300 °C from ZrCl<sub>4</sub>, Ta(OC<sub>2</sub>H<sub>5</sub>)<sub>5</sub> and O<sub>3</sub>. Ta<sub>2</sub>O<sub>5</sub> films were mixed with ZrO<sub>2</sub>, with Zr to Ta cation ratio of 0.8, being the total film thickness 25 nm. For electrical measurements, Al/Ti/Ta<sub>2</sub>O<sub>5</sub>:ZrO<sub>2</sub>/TiN/Si/Al capacitor stacks were constructed. Double-layer 110 nm/50 nm thick Al/Ti top

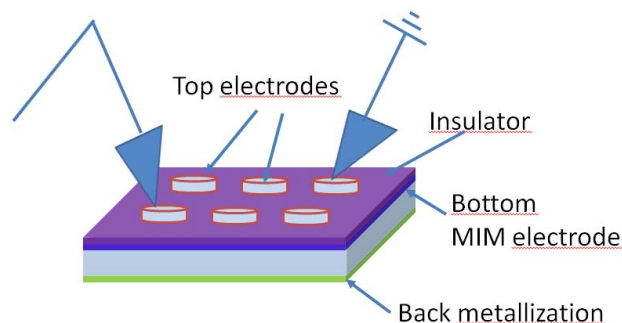


Fig. 1. Electrical connection setup.

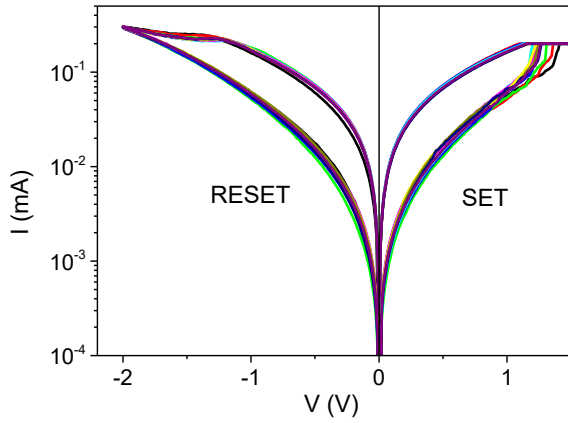


Fig.2. Bipolar I-V switching loops of  $Ta_2O_5$ - $ZrO_2$  MIM capacitors.

electrodes were evaporated through a shadow mask by electron beam evaporation, the Ti layer being in direct contact to  $Ta_2O_5:ZrO_2$  film. Top electrode area was  $0.204 \text{ mm}^2$ . Backside ohmic contact was provided by evaporating 100–120 nm thick Al layer on etched Si.

Electrical measurements showed in this work were carried out by means of a semiconductor analyzer (Keithley 4200SCS), with samples put in a light-tight and electrically shielded box. In order to avoid possible parasitic effects of the stacked layers in the bulk, the voltage was applied between two different top electrodes (see Fig.1). One of the samples is broken, so it behaves as a short circuit. The electrical behavior of the second one is then studied.

### III. EXPERIMENTAL RESULTS

The samples under study don't need a previous electroforming process to form the conductive filaments and activate the switching properties. By applying a voltage ramp of positive voltages with a current limitation of 0.2 mA, the low resistance state is reached (set process). In order to drive the sample back to the high resistance state, a decreasing voltage ramp is applied, from positive values to negative ones. For the reset process the current limitation was set at 0.5 mA, but it was never reached. That way, bipolar current-voltage switching loops with good repetitiveness were achieved (Fig.2). Devices are operated with a small voltage of less than  $|2| \text{ V}$ .

Similarly to I-V curves, both the real and the imaginary components of the admittance show hysteretic cycles. Measurements were carried out by superimposing a 100 kHz, 30 mV rms-ac signal to the DC bias voltage.

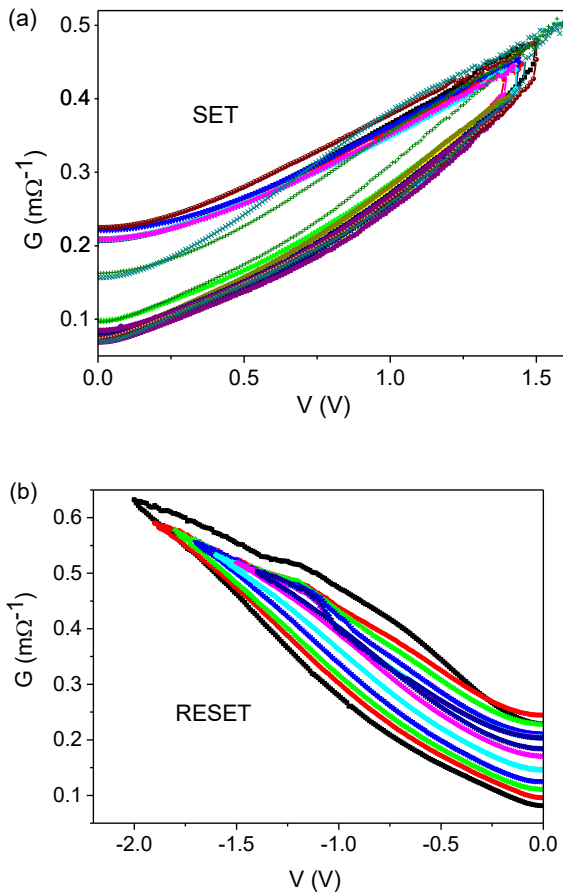


Fig.3. Conductance loops of  $Ta_2O_5$ - $ZrO_2$  MIM capacitors obtained by varying the voltage sweep extend for positive (a) and negative (b) voltages.

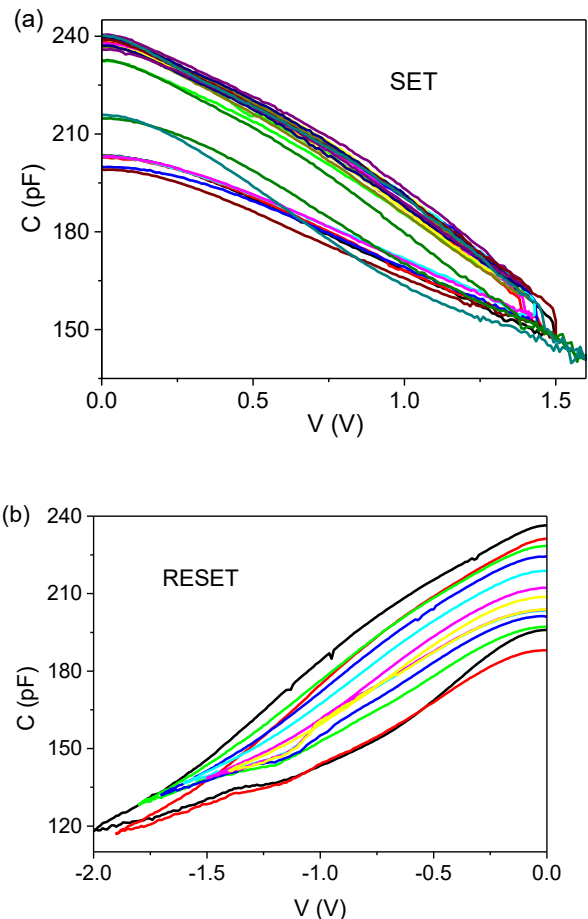


Fig.4. Capacitance loops of  $Ta_2O_5$ - $ZrO_2$  MIM capacitors obtained by varying the voltage sweep extend for positive (a) and negative (b) voltages.

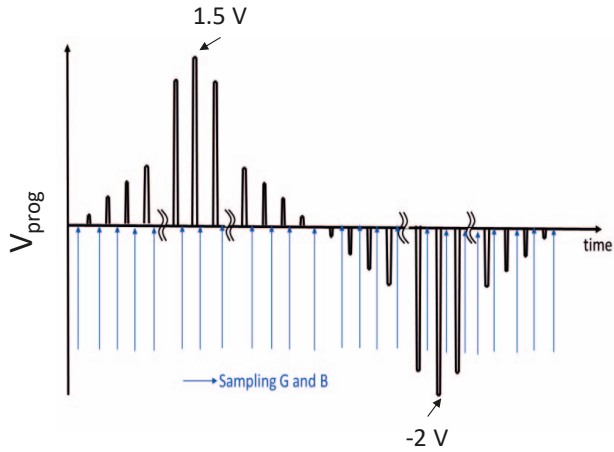


Fig. 5. Return to zero pulse voltage sequence used to measure the capacitance and conductance voltage at zero volts after a programming voltage,  $V_{prog}$ , ranging from -2 to 1.5 V.

In the set region the bias voltages applied were double linear ramps as follows:  $0\text{ V} \rightarrow -2\text{ V} \rightarrow 0\text{ V}$  (full reset),  $0\text{ V} \rightarrow V_{set} \rightarrow 0\text{ V}$ ,  $0\text{ V} \rightarrow -2\text{ V} \rightarrow 0\text{ V}$  (full reset), with  $V_{set}$  a positive voltage varying between 0 and +1.5 V, which is the value that leads to complete set.

In the reset region measurements were carried out in a similar way:  $0\text{ V} \rightarrow +1.5\text{ V} \rightarrow 0\text{ V}$  (full set),  $0\text{ V} \rightarrow V_{reset} \rightarrow 0\text{ V}$ ,  $0\text{ V} \rightarrow +1.5\text{ V} \rightarrow 0\text{ V}$  (full set), with  $V_{reset}$  a negative voltage between 0 and -2 V (complete reset).

The conductance-voltage and capacitance-voltage switching loops are depicted in Fig.3 and Fig.4, respectively. We see that depending on the amplitude of the voltage swing (that is, the values of  $V_{reset}$  on Fig.3 and  $V_{set}$  on Fig.4) the capacitance and conductance loops are inside those obtained when full reset or full set is applied (main loops). A great deal of internal loops inscribed within the main loop can be recorded. Excellent control of intermediate states was demonstrated.

In order to study the memory behavior, a return-to-zero pulse voltage sequence,  $0\text{ V}$  (1 ms)  $\rightarrow V_{prog}$  (1 ms)  $\rightarrow 0\text{ V}$  (1 ms), was used, with  $V_{prog}$  following a double ramp ranging between -2 to +1.5 V (see Fig. 5). Both conductance and capacitance are recorded at 0 V to discard any disturbance of the measurement process in the conductive filaments responsible of the conduction. In Fig.6 (a) and (b) memory cycles are shown. Both for conductance and capacitance two different states are clearly distinguished. Set and reset processes are produced at around +1.5 V, and -2 V, respectively, which exactly matches with I-V experiments.

#### IV. DISCUSSION

These loops provide detailed information about set and reset processes. In particular, reset process seems to be more complex than the set one. Indeed, a sharp increase of conductance signal (and, in correlation, a sharp decrease of capacitance signal) is produced just before the reset process takes place. These peaks of conductance and capacitance must be correlated with the very nature of the conductive filaments dynamic. In fact, as it has

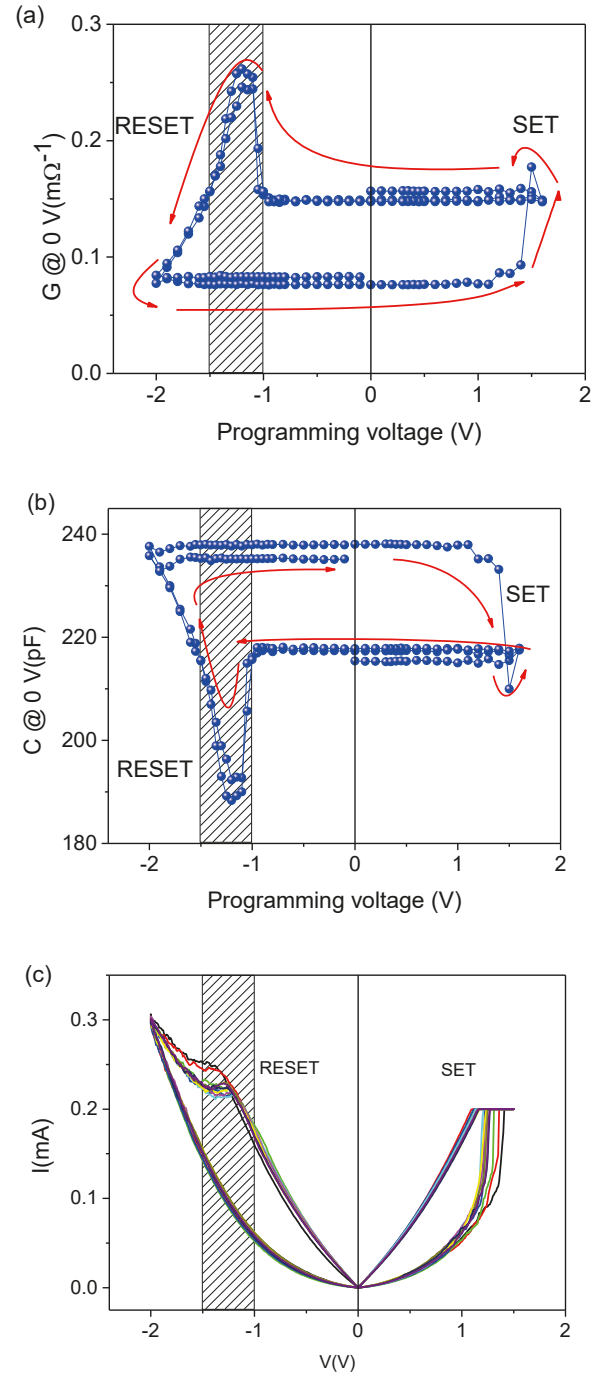


Fig. 6. Conductance (a) and capacitance (b) measured at 0 Volts as a function of the previous programming voltage. (c) DC current switching loops in linear scale

been stated (2, 12), the conductive filaments in this kind of materials are formed due to the accumulation of oxygen vacancies, which cluster, so connecting top and bottom electrodes (set process). When a positive bias is applied to the top electrode, Ta-O and Zr-O bonds break and  $O^{2-}$  ions migrate towards the top electrode/dielectric interface, leaving behind oxygen vacancies that will form the Ta and Zr rich conduction

path. A negative bias produces the reverse process, in which oxygen anions backfill the vacancies to annihilate the conductive path. Hence, the partial dissolution of filaments causes the reset process. Oxygen ions movement is due to the electrical field and Joule heating (13). From our measurements of admittance it seems that the filaments are reinforced just before dissolving. The conductance at 0 Volts quickly increases after programming voltages of about -1 V are applied and, correspondingly, the capacitance decreases. More negative programming voltages make both conductance and capacitance to return to the reset state values. To explain that we consider the fact that two metallic species are present in the dielectric composition: tantalum and zirconium. At the set state, oxygen vacancies appear in both Ta and Zr sites. When the reset process begins, oxygen vacancies on Ta sites are first occupied. Occupied Ta oxide may locally interchange charge with ionized Zr sites, yielding an additional conductance component,  $\Delta G$ . The relationship  $\Delta G/G_{\text{set}}$  is of around 0.8, which is equal to the Zr/Ta composition ratio. When more negative voltages are applied, the Zr sites are oxidized as well and, i.e., the above-mentioned mechanisms gradually disappear. Finally, G and C reaches their reset values.

Current loops in linear scale (Fig. 5c) provide a better view, and clearly show that the switching mechanism is not symmetrical: the set process is steep, whereas the reset one is gradual. Therefore, setting a current compliance for positive voltages is a main concern in order to avoid the hard breakdown of the structure. At the same time, the current compliance makes stronger the filament, hence higher  $V_{\text{reset}}$  values are needed to produce the reset (12). Due to the fact that the reset process is gradual, the stop voltage with negative polarity plays a more important role than the reset voltage in the complete rupture of the conductive filament (4). Indeed, for negative voltages it is possible to distinguish two different regions. At relatively low voltages, the conductive filament is still formed, and the current increases almost linearly with the bias voltage. With the increase of the negative bias, a considerable Joule heat is generated along with the increasing current. At around -1.2 V, the joint action of the negative electric field and the Joule heating activates the oxygen anion movement from the top electrode to the insulator bulk, starting the dissolution of the upper end of the conductive filament. Possibly a tunnel mechanism might be activated simultaneously, as the current strongly increases and becomes non-linear. When voltage bias reaches -2 V the current goes down, switching the device to its high resistance state.

## V. CONCLUSIONS

The study of admittance parameters provided a deep insight of the resistive switching behavior of Ta<sub>2</sub>O<sub>5</sub>:ZrO<sub>2</sub>-based MIM devices. Excellent control of internal loops of capacitance and conductance was achieved, which open its use in the neuromorphic and analog fields. The graphs of capacitance and conductance sensed at 0 V as a function of the programming voltage contain relevant information related to the switching mechanism. They can generate an effective fingerprint of each particular structure.

## ACKNOWLEDGMENT

This study has been supported by the Spanish TEC2014 under Grant No. 52152-C3-3-R, and by Finnish Centre of Excellence in Atomic Layer Deposition (Academy of Finland, 284623) and Estonian Academy of Science (SLTFYUPROF).

## REFERENCES

- [1] L. Zhang, R. Huang, M. Zhu, S. Qin, Y. Kuang, D. Gao, C. Shi, and Y. Wang, "Unipolar TaO<sub>x</sub>-based resistive change memory realized with electrode engineering", *IEEE Electron Dev. Lett.* vol. 31, no. 9, pp: 966-968, 2010.
- [2] S. Maikap, D. Jana, M. Dutta, and A. Prakash, "Self-compliance RRAM characteristics using a novel W/TaO<sub>x</sub>/TiN structure", *Nanoscale Res. Lett.* vol. 9, pp. 292-297, 2014.
- [3] M. Yu, Y. Cai, Z. Wang, Y. Fang, Y. Liu, Z. Yu, Y. Pan, Z. Zhang, J. Tan, X. Yang, M. Li, and R. Huang, "Novel vertical 3D structure of TaO<sub>x</sub>-based RRAM with self-localized switching region by sidewall electrode oxidation", *Sci. Rep.* vol. 6, p. 21020, 2016.
- [4] Z. Wang, J. Kang, Z. Yu, Y. Fang, Y. Ling, Y. Cai, R. Huang, and Y. Wang, "Modulation of nonlinear resistive switching behavior of a TaO<sub>x</sub>-based resistive device through interface engineering", *Nanotechnology*, vol. 28, p. 055204, 2017.
- [5] K. Chen, M. Nielsen, G. R. Yang, E. J. Rymaszewski, and T. M. Lu, "Study of amorphous Ta<sub>2</sub>O<sub>5</sub> thin films by DC magnetron reactive sputtering", *J. Electron. Mat.* Vol. 26, No.4, pp: 397-401, 1997.
- [6] B. C. Lai, N. Kung, and J. Y. Lee, "A study of the capacitance-voltage characteristics of metal-Ta<sub>2</sub>O<sub>5</sub>-silicon capacitors for very large scale integration metal-oxide-semiconductor gate oxide applications", *J. Appl. Phys.* vol. 85, No. 8, pp: 4087-4090, 1999.
- [7] K. Kukli, M. Kemell, M. Vehkamäki, M. J. Heikkilä, K. Mizohata, K. Kalam, M. Ritala, M. Leskelä, I. Kundrata, and K. Fröhlich, "Atomic layer deposition and properties of mixed Ta<sub>2</sub>O<sub>5</sub> and ZrO<sub>2</sub> films", *AIP Advances*, vol. 7, p. 025001 (15p), 2017.
- [8] H. Castán, S. Dueñas, A. Sardiña, H. García, T. Arroval, A. Tamm, T. Jogiias, K. Kukli, and J. Aarik, "RRAM memories with ALD high-k dielectrics: electrical characterization and analytical modeling", in *Thin Film Processes- Artifacts on Surface Phenomena and Technological Facets*, Chap. 9. Ed. Intech. ISBN: 978-953-51-3067-3, 2017, pp: 165-178.
- [9] L. Quingjiang, A. Khiat, I. Salaoru, C. Papavassiliou, X. Hui, and T. Prodromakis, "Memory impedance in TiO<sub>2</sub> based metal-insulator-metal devices", *Sci. Rep.* vol. 4, p. 4522, 2014.
- [10] T. Wakrim, C. Vallée, P. Gonon, C. mannequin, and A. Sylvestre, "From Memristor to Memimpedance device", *Appl. Phys. Lett.* vol. 108, N° 5, p. 053502, 2016.
- [11] S. Dueñas, H. Castán, H. García, E. Miranda, M.B. González, and F. Campabadal, "Study of the admittance hysteresis cycles in TiN/Ti/HfO<sub>2</sub>/W-based RRAM devices", *Mic. Eng.* Vol. 178, pp: 30-33, 2017.
- [12] B. Hudec, A. Paskaleva, P. Jancovic, J. Dérer, J. Fedor, A. Rosová, E. Dobrocka, and K. Fröhlich "Resistive switching in TiO<sub>2</sub>-based metal-insulator-metal structures with Al<sub>2</sub>O<sub>3</sub> barrier layer at the metal/dielectric interface", *Thin Solid Films.* Vol. 563, pp: 10-14, 2014.
- [13] J.-Y. Chen, C.-W. Huang, C.-H. Chiu, Y.-T. Huang, and W.-W. Wu, "Switching kinetic of VCM-based memristor: evolution and positioning of nanofilament", *Advanc. Mat.* Vol. 27, pp: 5028-5033, 2015.